MATERIALS SCIENCE

Biointerface mineralization generates ultraresistant gut microbes as oral biotherapeutics

Zhongmin Geng[1,2,3], Xinyue Wang[1], Feng Wu[1]*, Zhenping Cao[1]*, Jinyao Liu[1]*

Despite the fact that oral microecologics are effective in modulating the gut microbiome, they always suffer from multiple insults during the journey from manufacture to arrival at the intestine. Inspired by the protective mechanism of mineralization, we describe a cytocompatible approach of biointerface mineralization that can generate an ultraresistant and self-removable coating on bacterial surface to solve these challenges. Mineral coating endows bacteria with robust resistances against manufacture-associated oxygen exposure, ultraviolet irradiation, and 75% ethanol. Following oral ingestion, the coating is able to actively neutralize gastric acid and release encapsulated bacteria through spontaneous yet rapid double-decomposition reaction. In addition to acid neutralization, the generated calcium ions can trigger micellar aggregation of bile acid, enabling dual exemptions from the insults of gastric acid and bile acid to achieve uncompromised bacterial viability. Further supported by the therapeutic efficacy of coated bacteria toward colitis mice, biointerface mineralization provides a versatile platform for developing next-generation living oral biotherapeutics.

INTRODUCTION

The gut microbiome, which consists of a huge community of microorganisms, has been proved to be critical for maintaining host health (*1*). Intensive studies have disclosed that the disruption of gut microbial balance can cause compromise of intestinal homeostasis and subsequent onset of a broad variety of diseases (*2*). Supplementation with beneficial microbes has been commonly applied as an appealing strategy to prevent and treat diseases as the introduced species can reduce pathogen colonization and maintain a healthy microbial composition (*3*). With remarkable patient compliance, oral delivery of probiotic bacteria to the gut microbiome has been the most attractive supplementation approach due to its noninvasiveness (*4*). A key step toward the effectiveness of microbial biotherapeutics is the requirements of being viable during manufacture and remaining sufficient number following oral delivery to the intestine (*5*). Therefore, protective methods are urgently needed for preparing oral living biotherapeutics.

The formulations of dry powder, enteric coatings, and pills and the addition of milk whey, glycerol, trehalose, pepsin, and other protecting agents have been exploited to diminish environmental threats against bacterial therapeutics (*6*–*9*). Individual encapsulation using alginate, chitosan, cellulose, metal-phenolic networks, and metal-organic frameworks has been explored as an effective tool to physically shield bacteria from external attacks (*5*, *10*–*14*). More recently, we, along with other groups, have designed and prepared several coatings to minimize bacterial cell death and maximize bioavailability during oral delivery (*15*–*20*). For instance, coating with an extra self-assembled lipid membrane endows bacteria with the ability to resist gastrointestinal relevant threats (*21*). However, oral biotherapeutics prepared by existing methods severely suffer from several inevitable difficulties through the entire journey from bacterial culture to arrival at the intestine for colonization, resulting in extremely low availability.

First, exposure to oxygen during manufacture can induce toxicity to the enzymes and nucleic acids of anaerobes, which represent the vast majority of beneficial microbes (*22*). Second, to ensure safety and reduce potential risk of contamination, therapeutic products often undergo sterilization processing, leading to cellular stress, alterations of cellular structure, and even bacterial cell death (*23*, *24*). Last, after oral ingestion, intraluminal insults associated with the gastrointestinal tract, particularly gastric acid and bile acid, can deactivate the ingested microbes and cause insufficient number of viable cells at the time of arriving at the gut (*25*). Therefore, a method capable of protecting microbes during the whole process from manufacture to their arrival at the intestine for colonization is highly desirable. Unfortunately, to the best of our knowledge, this has not been reported yet.

In nature, the process of living organisms producing tough coatings to provide exoskeletal protection and support for soft tissue, which is termed mineralization, plays key roles in the survival of biosystems (*26*). Inspired by this natural phenomenon, various elegant biomimetic systems have been fabricated for drug delivery, biochemical separations, biomedical implants, and others (*27*, *28*). Here, we report an electrostatic interaction–mediated biointerface mineralization that forms an ultraresistant and self-removable coating on bacterial surface to tackle these difficulties (Fig. 1A). This method is applicable for coating diverse strains including both obligate and facultative anaerobes and has negligible influence on bacterial viability. Acting as a physical barrier, the resulting mineral coating confers encapsulated anaerobes with robust resistances to oxygen exposure, ultraviolet (UV) irradiation, and 75% ethanol associated with manufacture and product sterilization (Fig. 1B). Following oral ingestion, the coating can spontaneously react with gastric acid via double decomposition, simultaneously enabling rapid neutralization of gastric acid and adaptable release of encapsulated bacteria (Fig. 1C). Together with micellar aggregation of bile acid triggered by demineralization-generated calcium

[1]Shanghai Key Laboratory for Nucleic Acid Chemistry and Nanomedicine, Institute of Molecular Medicine, State Key Laboratory of Oncogenes and Related Genes, Shanghai Cancer Institute, Renji Hospital, School of Medicine, Shanghai Jiao Tong University, Shanghai 200127, China. [2]The Affiliated Hospital of Qingdao University, Qingdao University, Qingdao 266071, China. [3]Qingdao Cancer Institute, Qingdao University, Qingdao 266071, China.
*Corresponding author. Email: jyliu@sjtu.edu.cn (J.L.); caozhenping@renji.com (Z. C.); wufeng199001@163.com (F.W.)

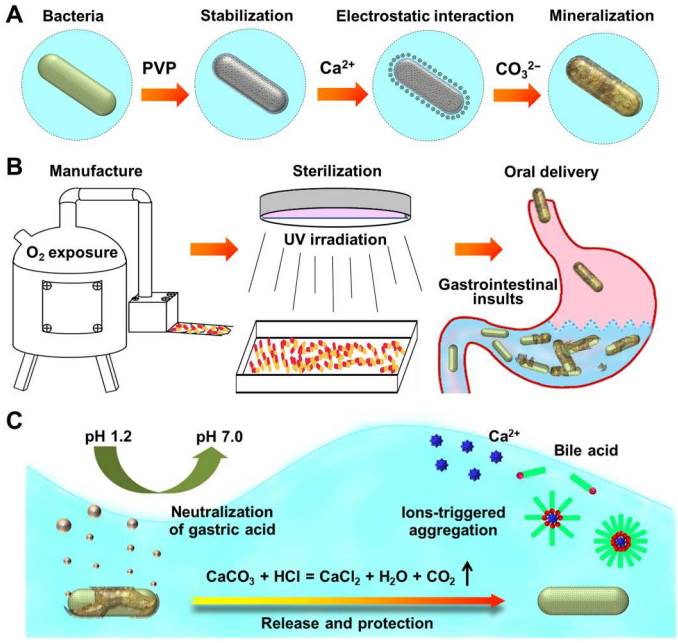

Fig. 1. Schematic illustration of biointerface mineralization that generates ultraresistant gut microbes as oral biotherapeutics. (**A**) Preparation of mineral coating on bacterial surface. (**B**) Resistances of coated bacteria against environmental assaults. (**C**) Neutralization of gastric acid, adaptable release of coated bacteria, and calcium ions–triggered aggregation of bile acid by double-decomposition reaction of mineral coating in the gastrointestinal tract following oral ingestion.

ions, protected bacteria are able to be exempted from dual insults of gastric acid and bile acid and arrive at the intestine with uncompromised cell viability. We show that a probiotic strain demonstrates its therapeutic potential against colitis in a dextran sulfate sodium (DSS)–induced murine model after coating with a mineral layer. Given its facile preparation and favorable biocompatibility, biointerface mineralization paves an avenue for developing innovative bacterial-based oral biotherapeutics.

RESULTS AND DISCUSSION

Design, preparation, and characterization of mineral coating

As a proof-of-concept study, we chose *Bacteroides fragilis* (BF839), a human commensal Gram-negative obligate anaerobe, which has been recognized as one of potential next-generation probiotics because of the ability to alleviate inflammation-associated diseases (*29*). To prepare calcium carbonate–coated BF839, we used a surfactant of polyvinyl-pyrrolidone (PVP) as a stabilizer to prevent bacterial aggregation by binding with negatively charged cell surface through electrostatic interactions. Meanwhile, after adequately mixing with calcium chloride via gentle shaking, calcium ions were absorbed onto the surface of PVP-stabilized BF839 cells by complexing with the introduced pyrrolidone groups. Upon the addition of sodium carbonate, the absorbed calcium ions guided the heterogeneous nucleation and deposition of calcium carbonate on BF839 cell surface to form a mineral coating. The synthesis of inorganic-organic hybrids by mimicking biomineralization is a process of heterogeneous nucleation, which forms bonding at the interface between bacterial cell wall and mineral crystals (*30*, *31*). Typically, the electrostatic interaction, polar interaction, and stereochemical recognition between inorganic crystals and organic matrix favor the heterogeneous nucleation of mineral crystals. The proposed mechanism for calcium carbonate deposition was depicted in fig. S1. First, abundant hydroxyl groups associated with peptidoglycan on bacterial cell wall have a strong interaction with the group of C═O in PVP through hydrogen bonding, which ensures the uniform distribution of PVP on the surface of bacteria. Then, the presence of N─C═O in PVP promotes the absorption of Ca^{2+} on bacteria surface by ion-polar interaction. Last, upon the addition of Na_2CO_3 aqueous solution, CO_3^{2-} easily integrates with Ca^{2+} by electrostatic interaction to form $CaCO_3$ nucleation sites. Therefore, bacteria can be uniformly coated via a mineralization process on their surface. The prepared coated BF839 were purified by centrifugation.

To confirm the obtained structure, we observed coated bacteria by transmission electron microscopy (TEM), which showed a rough surface with much higher contrast in comparison to native bacterial cells (Fig. 2A). Scanning electron microscopy (SEM) images exhibited that individual BF839 cells were encapsulated entirely after biointerface mineralization (Fig. 2B). Elemental mapping of coated bacteria was analyzed using energy-dispersive x-ray spectroscopy, illustrating that calcium signal was distributed uniformly over the entirely coated BF839 (fig. S2A). The presence of a mineralized layer was further verified by Fourier transform infrared (FTIR) spectra, where coated BF839 only featured the major absorbance regions of $CaCO_3$ (Fig. 2C). To further confirm the formation of calcium carbonate and its crystallographic structure, we applied both x-ray powder diffraction (XRD) and Raman spectroscopy. As indicated in fig. S2 (B and C), characteristic signal peaks assigned to the calcite phase were observed in both the Raman spectrum and XRD pattern of mineralized bacteria, verifying the formation of calcite-type calcium carbonate coating. The zeta potential of BF839 measured by dynamic light scattering (DLS) after interaction with PVP showed a clear increase from −37.8 ± 1.7 to −25.5 ± 2.7 mV, which further increased to near positive upon calcium ion absorbance (Fig. 2D). Following surface mineralization, the zeta potential decreased to −13.4 ± 0.8 mV, indicating the successful formation of a coating structure. We also labeled the mineral coating with calcein by coordination with calcium ions (*32*). Flow cytometry histogram of labeled coated bacteria displayed a notable increase in fluorescence intensity over both BF839 and BF839 mixed with calcein (Fig. 2E). Quantitative analysis of the ratio of fluorescent bacteria by flow cytometry suggested a coating efficiency of 88.2%. Laser scanning confocal microscopy (LSCM) images showed bright-green fluorescence signal by staining with calcein (Fig. 2F). Note that calcein containing a tetradentate ligand with four carboxyl groups can specifically bind with Ca^{2+}, forming a chelate. Meanwhile, calcein acetoxymethyl ester (calcein-AM) that needs to be converted into calcein to bind with Ca^{2+} by intracellular esterase was supplemented as a control to investigate calcium deposition. As shown in fig. S2D, typical LSCM images displayed negligible fluorescence signal, suggesting that calcein staining was attributed to extracellular calcium deposition. These results demonstrated the generation of a $CaCO_3$ coating on BF839 cell surface. It was worth mentioning that replacing calcium chloride with calcium lactate or calcium citrate was found to be difficult to form a mineral

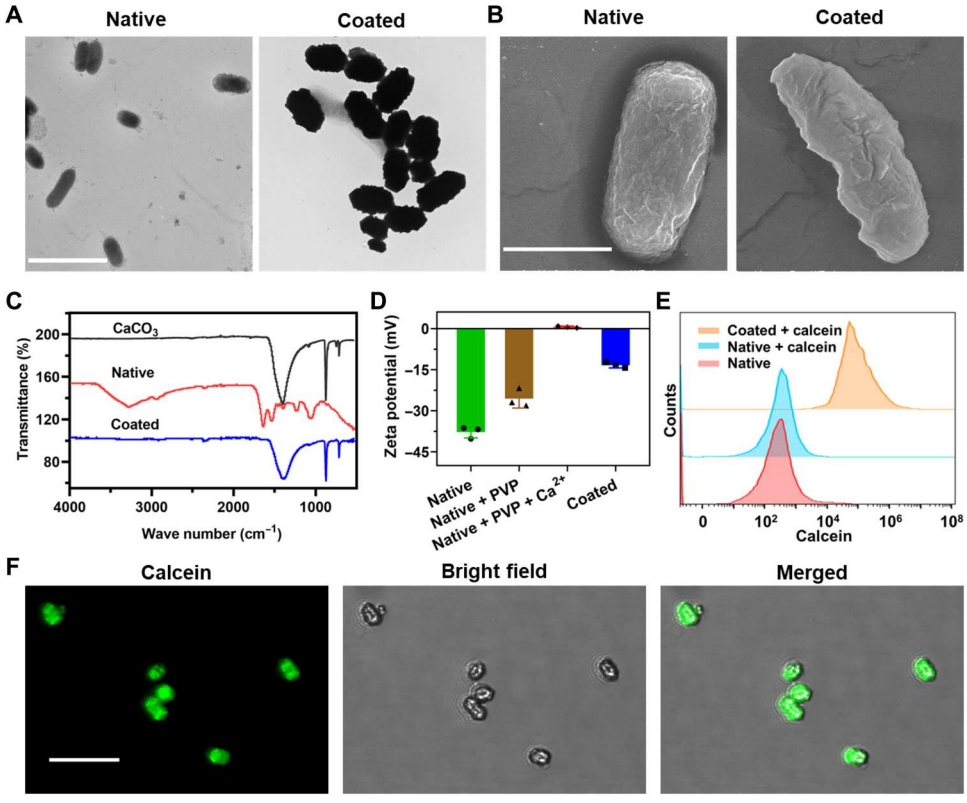

Fig. 2. Characterization of mineral coating. (**A**) Representative transmission electron microscopy (TEM) images of native BF839 and coated BF839. Scale bar, 5 μm. Sample suspensions were dropped onto Formvar/carbon 200-mesh grids, washed twice by double-distilled H_2O, and air-dried before observation. (**B**) Typical SEM images of native and coated BF839. Scale bar, 1 μm. Samples were fixed in 2.5% glutaraldehyde, serially dehydrated in ethanol, and coated with the help of a sputtering coater before observation. (**C**) FTIR spectra of $CaCO_3$ and native and coated BF839. Bacteria were freeze-dried and recorded in a frequency range of 450 to 4000 cm^{-1} at room temperature. (**D**) Zeta potentials of BF839 after different treatments. Bacteria were dispersed in phosphate-buffered saline (PBS) and measured by DLS. Error bars represent the SD (n = 3 independent experiments). Data are presented as means ± SD. (**E**) Flow cytometry histograms of calcein-labeled coated BF839. Native BF839 and native BF839 incubated with free calcein were used as controls. (**F**) Confocal images of coated BF839. Green channel indicates mineral coating labeled with calcein. Scale bar, 8 μm.

coating on the surface of BF839 cells under the same experimental conditions (fig. S2E).

To evaluate whether mineralization could influence bacterial viability, we assessed the growth curves of coated BF839 in a culture medium of Glfu anaerobic medium (GAM) by recording the values of optical density at 600 nm (OD_{600}). As expected, as plotted in Fig. 3A, the results revealed that the proliferation of coated BF839 was fully inhibited, which was in stark contrast with uncoated BF839. The inhibition of BF839 growth was ascribed to the presence of a tough $CaCO_3$ layer that restrained both bacterial division and substance exchange for growth. Encouragingly, after demineralization of coated BF839 by hydrochloric acid (pH 4.0), the growth curve was found to be comparable to that of unmodified BF839, showing insignificant difference in cell viability between native and decoated bacteria. The bacterial viability of coated BF839 was further investigated by live/dead staining using a combination of calcein-AM and propidium iodide, followed by flow cytometric analysis. As shown in fig. S3 (A and B), the viability of decoated BF839 was comparable to that of native BF839, suggesting the uninfluenced viability of coated bacteria. Plate counting illustrated that the growth of coated BF839 was near completely suppressed in GAM, while the viabilities of native and decoated BF839 remained accordantly, further clarifying that both preparation procedures and the formation of a mineral coating played limited negative effects on bacterial activity (Fig. 3B and fig. S3C). Moreover, the viabilities of BF839 after treatments with equivalent PVP and $CaCl_2$ to mineralization process showed no notable differences compared to the viabilities of untreated bacteria (fig. S4A). As bacteria are able to switch its metabolism state to a dormant state by maintaining a low adenosine triphosphate (ATP) level for long-term survival upon exposure to stress conditions, including desiccation, nutrient starvation, and low oxygen (*33*), firefly luciferase–based ATP assay was performed to examine the ATP levels of coated bacteria. As confirmed in fig. S4B, BF839 after mineralization maintained a relatively low ATP level, which was about sixfold lower than that of uncoated bacteria. This result indicated the switch of BF839 to a dormant state after coating. In addition, we explored the versatility of interface mineralization to coat diverse strains. As given in Fig. 3 (C to F) and fig. S4C, TEM imaging together with zeta potential measurement claimed that facultative anaerobe *Escherichia coli* Nissle 1917 (EcN), obligate anaerobe *Bifidobacterium* (Bif), and *Lactobacillus rhamnosus* GG (LGG) could be similarly coated, highlighting the broad applicability of this method to mineralize different strains.

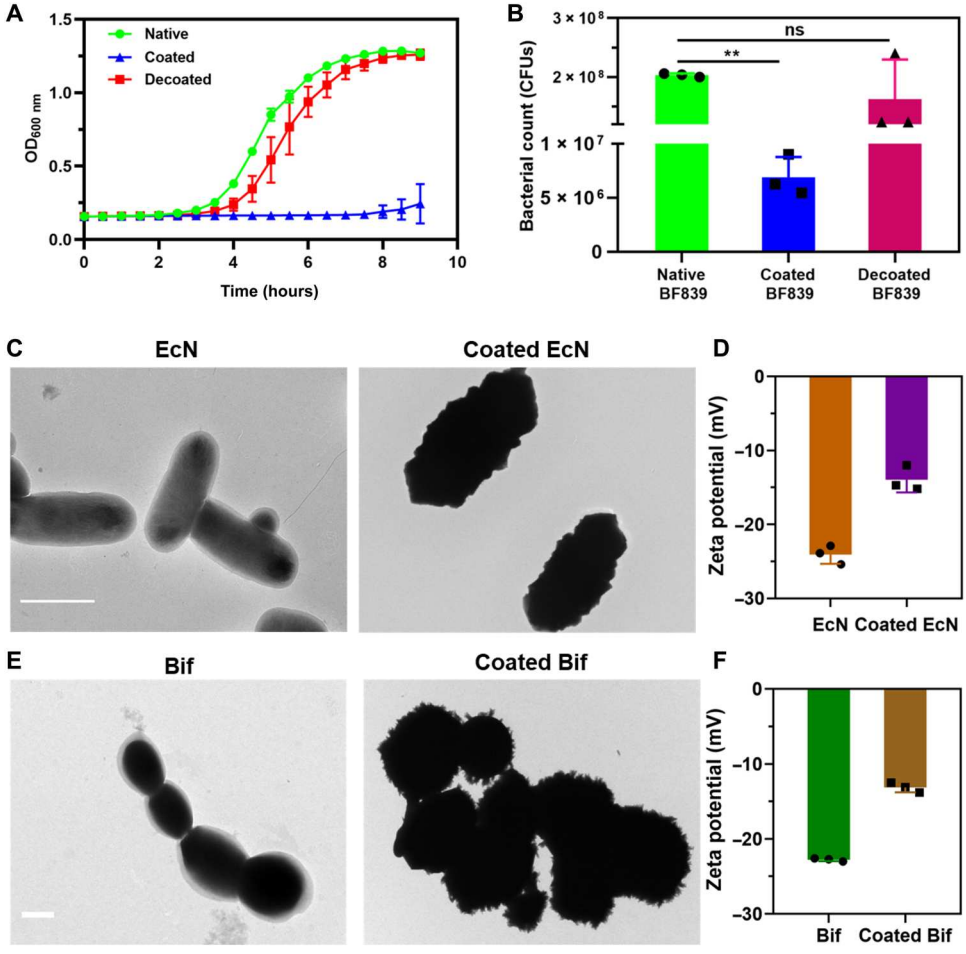

Fig. 3. Cytocompatibility and versatility of mineral coating. (**A**) Growth curves of native, coated, and decoated BF839 cultured in GAM broth at 37°C. OD_{600} was recorded at 30-min intervals using a microplate reader. (**B**) Cell viabilities of native, coated, and decoated BF839. Bacterial counts were determined by plate counting. Significance was assessed using one-way analysis of variance (ANOVA), giving *P* values: $^{**}P < 0.01$. ns, no significance. CFU, colony-forming units. (**C**) Representative TEM images of native and coated *Escherichia coli* Nissle 1917 (EcN). Scale bar, 2 μm. (**D**) Zeta potentials of native and coated EcN measured in PBS by DLS. (**E**) Typical TEM images of native and coated *Bifidobacterium* (Bif). Scale bar, 1 μm. (**F**) Zeta potentials of native and coated Bif measured in PBS by DLS. Error bars represent the SD ($n = 3$ independent experiments). Data are presented as means ± SD.

Resistances against manufacture-associated threads

We next studied the protection role of mineral coating in the survival and growth of coated BF839 under various stimulations associated with manufacture including air exposure, UV irradiation, and 75% ethanol. After fermentation process, bacteria inevitably suffer from air exposure during formulation preparation and packaging, in which oxygen can deactivate anaerobic species (*34*). As displayed in Fig. 4A, more than 75% of decoated BF839 survived after storage at 4°C for 30 days with exposure to air. However, an ignorable number of uncoated BF839 (less than six orders of magnitude) survived under the same experimental condition. Bacterial morphology visualized by TEM proved that the production of oxygen-induced cytoplasmic membrane vesicles and corresponding bubbling cell death were avoided in coated BF839 other than uncoated bacteria (Fig. 4B) (*35*). The improved tolerance to oxygen toxicity could be explained by the isolation effect of mineral layer on cell surface, which impeded the diffusion of oxygen molecule (*36*). UV irradiation, an external aggressor, can remarkably damage the structures of proteins and enzymes in bacteria (*14*). The resistance of coated BF839 against UV irradiation was investigated considering the fact that UV irradiation is widely used during manufacture processing and product sterilization of bacterial therapeutics (*37*, *38*). As depicted in Fig. 4C, the count of survived decoated BF839 had no notable decrease under UV irradiation (100 $\mu W/cm^2$) for 30 min. In contrast, nearly complete death was observed for uncoated BF839 under the same treatment, suggesting that $CaCO_3$ coating could shield the harmful effects of UV irradiation toward bacterial cells. TEM observation of native BF839 displayed the accumulation of cellular compounds (Fig. 4D), suggesting the deactivation of intracellular enzymes (*39*). Note that the occurred variation was not observed in irradiated coated BF839, further supporting the ability of mineral layer to protect encapsulated bacteria from UV sterilization (Fig. 4E). Alcohol, probably the most commonly used disinfectant, has strong bactericidal activity, which directly sterilizes bacteria by denaturing and dehydrating proteins (*40*). In the presence of a $CaCO_3$ coating, quantitative survival of decoated BF839 after direct incubation in 75% ethanol for 10 min achieved almost six orders of magnitude higher than that of uncoated bacteria (fig.

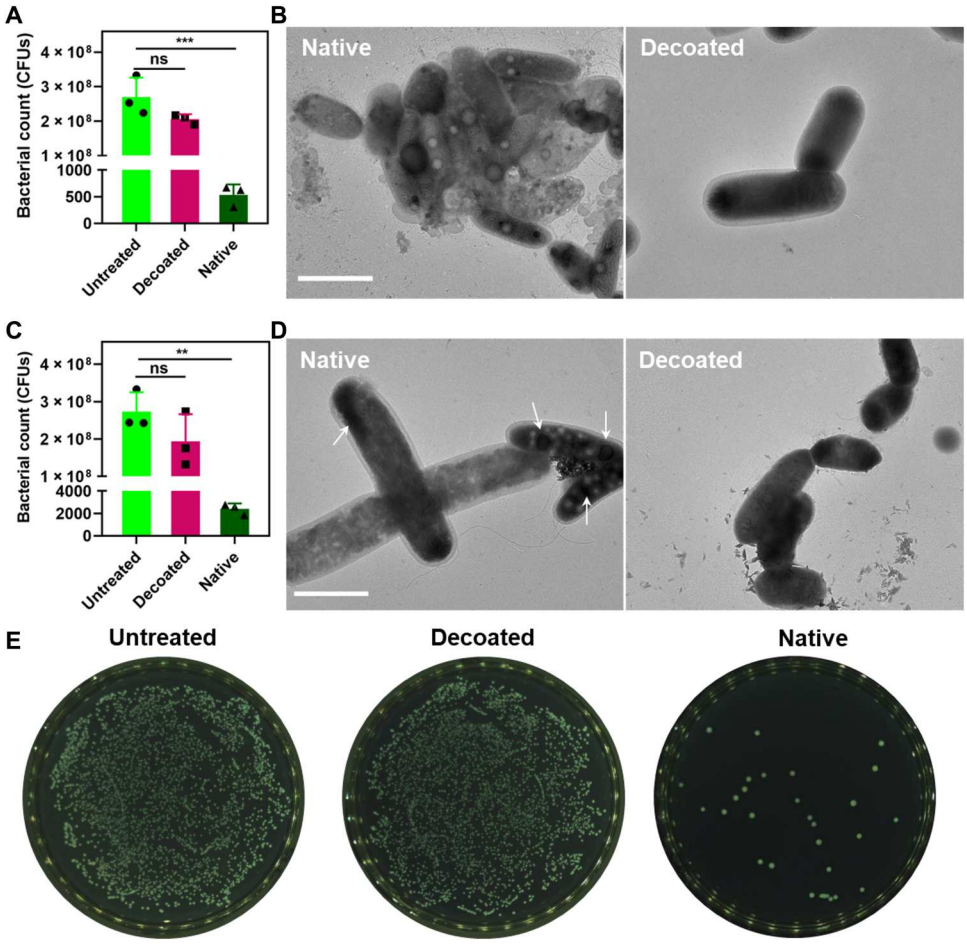

Fig. 4. Resistances against manufacture-associated threads. Equivalent native and coated BF839 were exposed to the following: (**A**) air for 30 days and (**C**) UV irradiation for 30 min. After the indicated time points, the numbers of bacteria were recorded by plate counting. Error bars represent the SD ($n = 3$ independent experiments). Data are presented as means ± SD. Significance was assessed using one-way ANOVA, giving P values: $^{**}P < 0.01$ and $^{***}P < 0.001$. (**B** and **D**) Representative TEM images of native and coated BF839 against air exposure and UV irradiation. White arrows indicate the area of accumulated cellular compounds. Scale bar, 2 μm. (**E**) Typical plates of decoated BF839 and native BF839 after exposure to UV irradiation for 30 min. Untreated native BF839 were used as a control. Agar plates were incubated at 37°C overnight before imaging.

S5A). TEM images certified that exposure to 75% ethanol disrupted or even dissolved bacterial envelope, resulting in the killing of uncoated BF839, while decoated BF839 retained their envelope structure and smooth cell surface unchanged because of the protection effects of mineral coating (fig. S5B). These data provided strong evidence that mineralization of bacteria greatly improved their resistance against manufacture-related environmental assaults.

Self-removability of mineral coating

The challenge of bacterial therapeutics encountered after oral ingestion is to survive gastric acid (pH 1 to 3) and bile acid in the upper gastrointestinal tract (*41*). We speculated that following oral delivery, the mineral layer of coated bacteria could actively react with gastric acid through double decomposition, which was able to neutralize intragastric acidic environment, while release encapsulated bacteria under a cytocompatible condition. As visualized in Fig. 5A, the generation of air bubbles immediately after mixing coated BF839 with simulated gastric acid (SGF; pH 1.2) and the completion of reaction in minutes suggested the decomposition of $CaCO_3$ coating. Figure 5B referred to a bacterial number–dependent pH neutralization process measured by adding a series of gradually increased amounts of coated BF839 into 20 ml of acid solution (pH 1.2). Upon mixing, spontaneous reaction of $CaCO_3$ coating with acid led to continuous increase of pH, which was markedly increased from 2 to 5.5 with bacterial number increasing from 23 $\times 10^8$ to 35 $\times 10^8$ colony-forming units (CFUs). This result affirmed the capacity of coated BF839 to efficiently neutralize acidic solution. We then examined the decoating of coated BF839 in SGF. Flow cytometric histograms of BF839 (1×10^8 CFUs) coated with a calcein-labeled mineral layer emerged a marked decrease in fluorescence intensity after incubation with 1.2 ml of SGF for 5 min (Fig. 5C). With SGF volume increasing to 2.4 ml, the mineral layer was decoated completely as the fluorescence intensity of coated bacteria decreased to a level similar to uncoated BF839. The shoulder in the histogram of 0-ml SGF might be ascribed to heterogeneous labeling after incubation and rinse. Coated BF839 after incubation with different volumes of SGF were also visualized by TEM. As illustrated in fig. S6A, obvious burrs were observed on the surface of

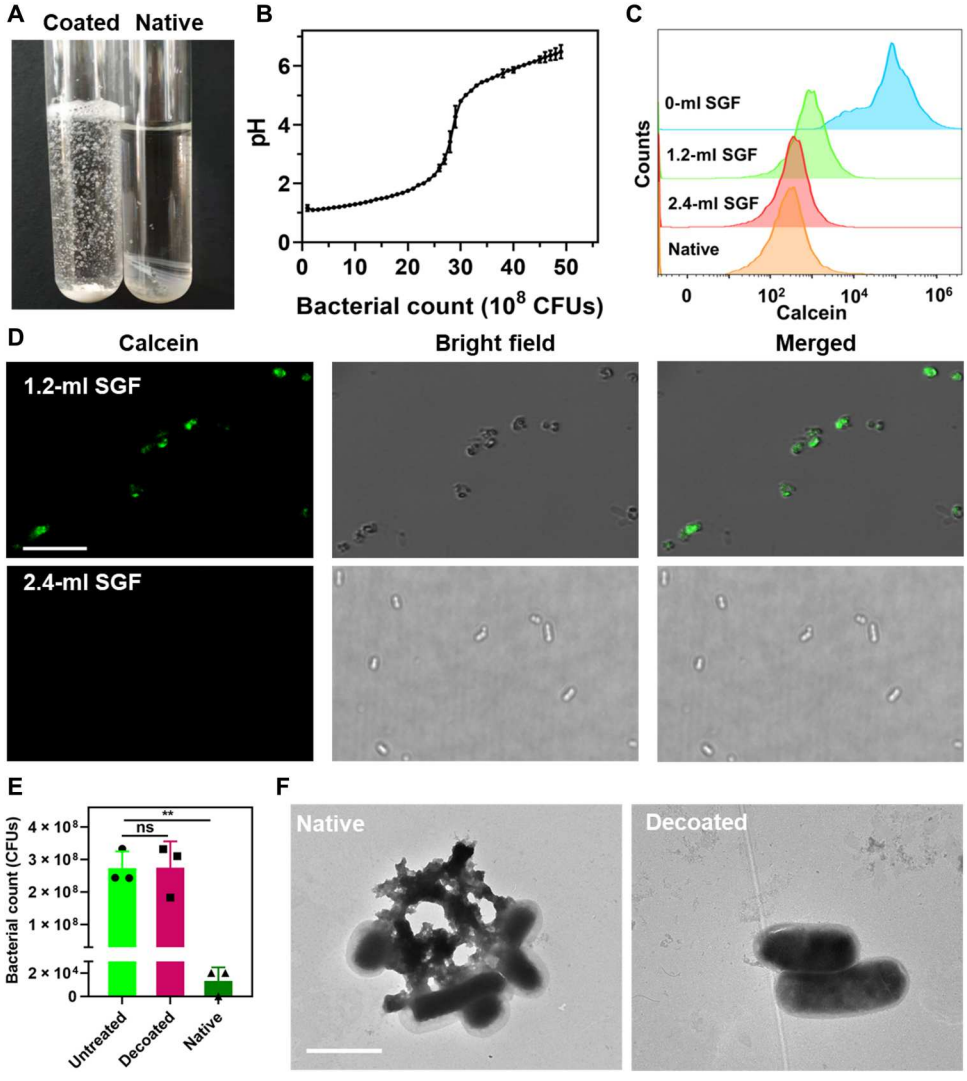

Fig. 5. Self-removability of mineral coating. (**A**) Digital photos of native and coated bacteria incubated with simulated gastric acid (SGF). Equivalent freeze-dried native and coated BF839 were added to 5 ml of SGF just before image capture. (**B**) Bacterial number–dependent pH neutralization measured by adding a series of gradually increased amounts of coated BF839 into 20 ml of SGF. (**C**) Flow cytometry histograms of bacteria after different treatments. Native BF839 was used as a control. A volume of 1.2 or 2.4 ml of SGF was added dropwise into 1×10^8 CFUs of calcein-labeled coated BF839, and the mixture was collected after incubation for 5 min and washed twice by PBS before analysis. (**D**) Confocal images of calcein-labeled coated BF839 after incubation with 1.2 or 2.4 ml of SGF for 5 min. Green channel refers to calcein-labeled mineral coating. Scale bar, 8 μm. (**E**) Numbers of survived bacteria. Equivalent native and coated BF839 were exposed to SGF for 2 hours, and the number of survived BF839 was calculated by plate counting. Native BF839 and untreated native BF839 were used as controls. Error bars represent the SD ($n = 3$ independent experiments). Data are presented as means ± SD. Significance was assessed using one-way ANOVA, giving P values: $^{**}P < 0.01$. (**F**) TEM images of native and coated BF839 after incubation with SGF. Scale bar, 2 μm.

coated BF839 after incubation. This result suggested the occurrence of double-decomposition reaction, in which the $CaCO_3$ coating was decomposed by the hydrochloric acid in SGF. With SGF volume increasing, the shedding of mineral coating could be observed. This could be explained by the observation that bacteria were able to proliferate once the coating turning into permeable. These results implied that the decoating of bacteria might not require the full decomposition of mineral coating, which was in good agreement with our previous work that the coating could be shed off by bacterial division (*42*). Acid-triggered removal of $CaCO_3$ layer was further visualized by LSCM, displaying a much weakened green fluorescence signal after SGF treatment and subsequently completes disappearance upon increasing the volume of used acidic solution (Fig. 5D). Encouraged by accordant results obtained from flow cytometry and LSCM measurements, we further assessed the number and viability of coated BF839 after SGF exposure. As expected, rare native BF839 survived successfully following 2-hour incubation in SGF at 37°C. Plate counting implied that coated BF839 remained almost the same bacterial number to that of untreated native BF839 (Fig. 5E). Quantitative counting verified that acid-mediated decomposition of $CaCO_3$ layer enabled a full decoating of coated BF839 and that the vitality of released bacteria remained uncompromised after undergoing SGF insult. TEM imaging illuminated that mineral coating around BF839 was dissolved by acid and that the

decoated bacteria presented smooth cell surface and normal envelope shape (Fig. 5F). In contrast, native BF839 that suffered from acidic insult arose with destructed bacterial cellular structure and even the leakage of intracellular components (*43*). It is worth mentioning that calcium ions generated from double-decomposition reaction were found to be able to trigger bile acid aggregation (*44*), which could diminish its toxicity to the released BF839 and therefore enhance their survival once entering the duodenum (fig. S6, B and C).

In vivo decoating and resistance

Having confirmed the self-removability of mineral coating in vitro, we turned our attention to validate its performance in vivo. To monitor the decoating of coated bacteria in gastric cavity, we orally gavaged 1×10^7 CFUs of bacteria coated with calcein-labeled mineral layer to mice and separately extracted intraluminal contents from the stomach and the intestine at 0, 1, and 5 hours after administration. Native bacteria were administered as a control. To track the demineralization of coated bacteria, we used EcN genetically engineered with mCherry expression and kanamycin resistance because of the ability to identify from endogenous gut microbiota by color and the growth in kanamycin-supplied LB medium (*45*). Notably, coated bacteria showed a reduction of calcein signal but an increase of mCherry signal in the contents of the stomach from 0 to 5 hours, proposing that demineralization occurred and released bacteria were protected from neutralized intragastric pH (Fig. 6A and fig. S7). On the contrary, a gradually disappearing of mCherry signal was observed for native bacteria, which was caused by the insult of gastric acid. Furthermore, compared to the native group, much more mCherry-marked bacteria were visualized in contents extracted from the intestine of the coated group at 1 and 5 hours after gavage, pointing out the enhanced survival of coated bacteria (fig. S8, A and B). One of the main mechanisms for the in vivo demineralization of coated bacteria was the occurrence of double decomposition triggered by gastric acid. Note that complete decomposition could be achieved in the gastric cavity by tuning the dose of coated bacteria basing on the result of titration. Another major cause for the decoating of bacteria could be the shedding enabled by bacteria division. As shown in fig. S8B, a number of calcein-labeled particles were visualized in the intestinal contents sampled at 1 and 5 hours after gavage, pointing out the shedding of mineral layers. To analyze the overall decoating and survival of bacteria in-situ, mice were orally delivered with 1×10^7 CFUs of luxCDABE-expressing EcN coated with a calcein-labeled mineral layer (*46*), and the gastrointestinal tract was harvested at 1 and 5 hours after ingestion for in vivo imaging system (IVIS) measurement. Representative IVIS images captured at predetermined time points showed an inverse relationship between luxCDABE luminescence and calcein fluorescence, declaring successful demineralization and survival of coated bacteria in the gastrointestinal tract (Fig. 6B and fig. S9), while, in the native group, the sampled tracts emitted negligible signal of luxCDABE luminescence, which in turn reflected the protective effects of mineral coating. To quantitatively determine the number of survived bacteria following oral delivery, intraluminal contents from both the stomach and the intestine were collected for plate counting. As validated in Fig. 6C, coated bacteria exhibited substantially promoted survivals in the stomach at 1 and 5 hours after administration, which were separately more than two and almost six times higher than those of native bacteria. Similarly, in comparison to the uncoated group, the survivals of coated bacteria were almost 5 and more than 4.5 times higher in the intestine, respectively (Fig. 6D). Together, double-decomposition reaction–mediated gastric acid neutralization and bacterial release demonstrated the resistance and self-removability of mineral coating to effectively protect coated bacteria from gastrointestinal stressors during oral delivery.

Potential therapeutic application of coated bacteria

To explore the potential application of this approach, we evaluated the efficacy of coated BF839 as an oral biotherapeutic for disease treatment. With increasing incidence, ulcerative colitis, one of the main types of inflammatory bowel diseases, has affected about 11.2 million people worldwide (*47*). Currently available therapies remain unsuccessful to control symptoms adequately in most patients, resulting in adversely affected quality of life (*48*). BF839 strain has been studied to treat DSS-induced colitis as the secretion of short chain fatty acids can improve its anti-inflammatory effects (*49*). Therefore, we investigated the potency of coated BF839 to treat colitis in a DSS-induced mouse model. Mice were fed with 3% DSS drinking water for a week to induce colitis (*50*) and then orally administered with coated BF839 daily for another 5 days (Fig. 7A). Healthy mice and DSS-induced mice treated with uncoated BF839, phosphate-buffered saline (PBS), and $CaCO_3$ were applied as controls, respectively. As shown in Fig. 7B, the body weight of mice was recorded every day, and the results indicated that DSS feeding induced continuous decrement in body weight as compared to that of healthy mice. Interestingly, DSS mice treated with coated BF839 recovered body weight more efficiently than those of uncoated BF839–, PBS-, and $CaCO_3$-treated groups. Average length of the intestinal tracts harvested and measured at day 5 after treatment suggested that DSS could induce reduction in intestinal length and the use of uncoated BF839 played moderate beneficial effect (Fig. 7, C and D). Encouragingly, the average length of the intestinal tracts sampled from coated BF839–treated mice approximated to that of healthy mice, which was notably larger than that of uncoated BF839–dosed mice. Furthermore, double-blinded enzyme-linked immunosorbent assay (ELISA) and myeloperoxidase (MPO) staining were conducted to assess the inflammatory level of colitis. Compared to those treated with uncoated BF839, PBS, and $CaCO_3$, the mice from the coated BF839–treated group had markedly reduced inflammatory responses, as proved by the lower level of tumor necrosis factor–α (TNF-α), one of the key inflammatory cytokines in serum (*51*) (Fig. 7E). Compared to healthy mice, a similar level of TNF-α was perceived in coated BF839–treated mice. In addition, the mean number of MPO-positive cells in colonic tissue sectioned from coated BF839–treated mice was greatly lower than those in all negative-control groups (Fig. 7, F and G). It was noted that typical images of hematoxylin and eosin (H&E) staining of the colon in coated BF839 group showed undetectable histological damages including shedding of mucosal epithelial cells and disappearance of missed intestinal glands in lamina propria, which were similar to those from healthy mice (Fig. 7H). In brief, coated BF839 verified potent therapeutic effects as supported by prolonged intestinal length, remitted inflammatory responses, and limited histological damages. The enhanced efficacy could be interpreted by mineral coating–enabled elevation of survival rate of coated bacteria.

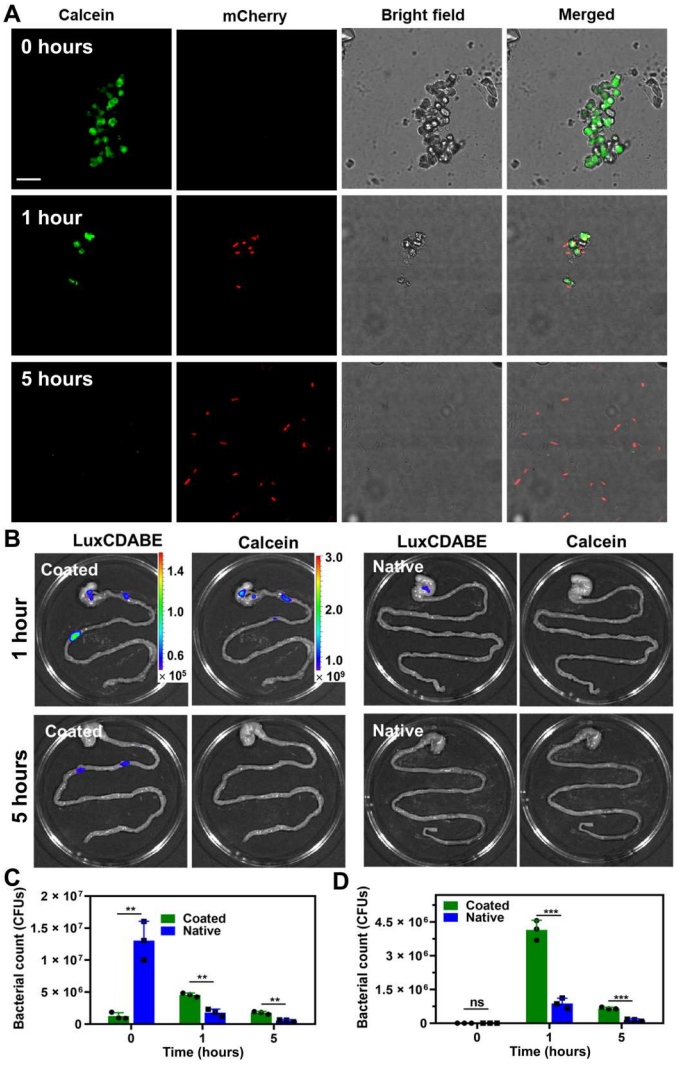

Fig. 6. In vivo decoating and resistance. (**A**) Confocal images of mCherry-expressing EcN coated with calcein-labeled mineral layer. Bacteria were separately collected from the gastric cavity of mice at 0, 1, and 5 hours after oral gavage of 1×10^7 CFUs of native or coated EcN. Green and red channels indicate calcein-labeled mineral coating and EcN expressing mCherry. Scale bar, 10 μm. (**B**) IVIS images of the gastrointestinal tracts harvested at 1 and 5 hours after administration of 1×10^7 CFUs of LuxCDABE-expressing native or calcein-labeled coated EcN. Color bar indicates luminescent (p s^{-1} cm^{-2} sr^{-1}) and fluorescent [(p s^{-1} cm^{-2} sr^{-1})/(μW cm^{-2})] radiance, respectively. Bacterial reservations in (**C**) the stomach and (**D**) the intestinal tract, respectively. At 0, 1, and 5 hours after gavage of 1×10^7 CFUs of native or coated EcN, intraluminal content of each mouse was collected for bacterial plate counting. Error bars represent the SD ($n = 3$ independent experiments). Data are presented as means ± SD. Significance was assessed using Student's t test, giving P values: $^{**}P < 0.01$ and $^{***}P < 0.001$.

In summary, to tackle the challenges of overall low availability of oral probiotic therapeutics, we have described a strategy to protect bacterial bioagents from external insults associated with manufacture to arrival at the intestine. Inspired by the protective effect of mineralization, a facile method of electrostatic interaction–assisted biointerface mineralization is developed to deposit an ultraresistant and self-removable coating for bacterial protection. This approach is versatile to coat diverse species including obligate and facultative anaerobes, and both preparation procedures and formed coating have negligible influences on bacterial viability. Because of its physical barrier role, the resultant single-cell coating endows individually wrapped anaerobes with robustness to resist insults associated with manufacture and product sterilization, including oxygen exposure, UV irradiation, and 75% ethanol. After oral ingestion, double-decomposition reaction that spontaneously occurred between mineral coating and gastric acid is able to achieve rapid neutralization of intragastric low pH and demineralization-triggered release of coated bacteria. Simultaneously, decomposition-produced calcium ions induce micellar aggregation of bile acid, leading to a dual exemption of released bacteria from the insults of gastric acid and bile acid for subsequent intestinal colonization. We show that with the help of a mineral coating, probiotic *B. fragilis* strain demonstrates an impressive therapeutic efficacy in a DSS-induced murine model of colitis. In consideration of its ability to codeposit other functional molecules, we anticipate that biointerface mineralization could open a window for preparing multifunctional bacterial-based bioagents for a broad variety of biomedical applications.

MATERIALS AND METHODS

Materials and strains

EcN, BF839, Bif, and LGG were obtained from China General Microbiological Culture Collection Center. GAM containing 1.0% (w/v) peptic digest of animal tissue, 0.3% papaic digest of soybean meal, 1.0% protease peptone, 1.35% digested serum, 0.5% yeast extract, 0.22% beef extract, 0.12% liver extract, 0.3% glucose, 0.25% potassium dihydrogen phosphate, 0.3% sodium chloride, 0.5% soluble starch, 0.03% L-cysteine hydrochloride, and 0.03% sodium thioglycollate and LB medium containing 1% bacto-tryptone, 0.5% yeast extract, 1% NaCl, and 0.1% glucose were purchased from Hope Bio-Technology Co., Ltd. (Shandong, China) and used as the medium for cloning. PBS was provided by Sigma-Aldrich (USA). Na_2CO_3, calcein, $CaCl_2$, and PVP with an average weight-average molecular weight of 44 kDa were obtained from Adamas-beta (Shanghai, China). Plasmids pBBR1MCS2-Tac-mCherry (kanamycin resistant), pMD18-luxCDABE (ampicillin resistant), and all other reagents were obtained from domestic suppliers and used as received. SGF (pH 1.2) was prepared by dissolving 3.2 g of pepsin and 2.0 g of NaCl in 1 liter of deionized water, followed by the addition of 7 ml of concentrated hydrogen chloride (HCl) solution and then adjusting the pH to 1.2 with diluted HCl solution. Subsequently, the obtained buffer was filtered by a 0.22-μm membrane. Bacteria were grown in GAM at 37°C with suitable antibiotics.

Animal studies

Female Institute of Cancer Research (ICR) mice (6 to 8 weeks, 17 to 20 g) and C57BL/6 female mice (6 to 8 weeks, 17 to 20 g) were provided by Jiesijie Laboratory Animal Center (Shanghai, China). Female mice have been widely used for DSS-induced colitis models given the robust immune responses to different chronic inflammatory diseases (*52*). All mice were housed and fed under 12-hour/12-hour dark/light cycle, specific pathogen–free conditions, an ambient temperature of 25°C, and a humidity of 55%. All animal experiments were performed under the guidelines evaluated and approved by the ethics committee of Institutional Animal Care and Use Committee of Shanghai Jiao Tong University.

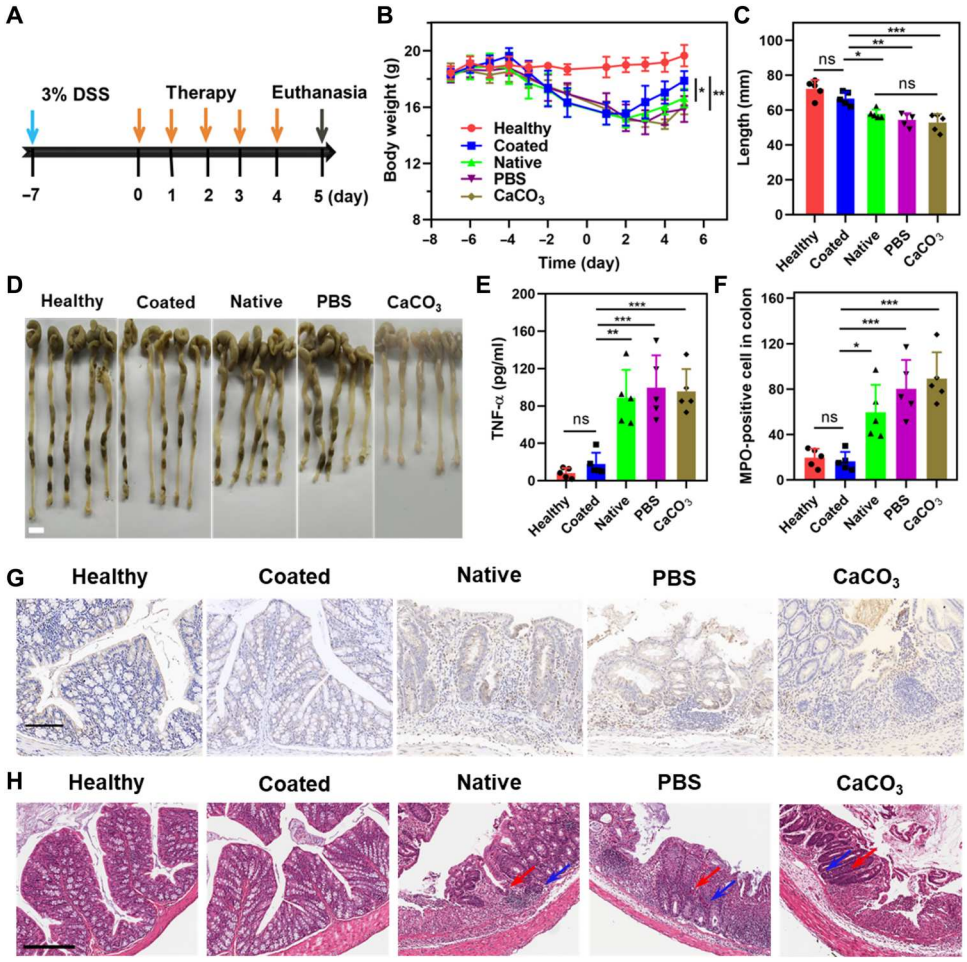

Fig. 7. Therapeutic application of coated bacteria. (**A**) Experimental design for colitis treatment. Mice were given with 3% DSS for 7 days to induce colitis and then daily administered with 1×10^7 CFUs of coated or native BF839 by oral gavage for another 5 days. PBS, $CaCO_3$, and healthy mice were used as controls, respectively. The intestinal tract of each mouse was harvested for double-blinded histopathological analysis 5 days after administration. (**B**) Variation of mouse body weight during infection and treatment. (**C**) Average lengths and (**D**) digital photos of the intestinal tract 5 days after treatment. Scale bar, 1 cm. (**E**) Serum level of TNF-α 5 days after treatment. (**F**) Mean MPO-positive cells counted in the colon. Representative images of (**G**) MPO and (**H**) H&E staining of the colon after treatment. Red and blue arrows represent epithelial injury and inflammation, respectively. Scale bar, 150 μm. Error bars represent the SD ($n = 5$ independent experiments). Data are presented as means ± SD. Significance was assessed using one-way ANOVA, giving P values: $^*P < 0.05$, $^{**}P < 0.01$, and $^{***}P < 0.001$.

Growth of bacteria

EcN carrying pBBR1MCS2-Tac-mCherry or pMD18-luxCDABE were grown at 37°C overnight in 10 ml of liquid LB medium with supplement of kanamycin (50 μg/ml). BF839 were grown at 37°C in bacteroides phage recovery medium broth in an anaerobic glove box. Bif were grown at 37°C in bifidobacterium BS medium in an anaerobic glove box. Overnight culture was diluted 1:50 (v/v) to fresh LB liquid medium and grown at 37°C for 2 to 3 hours. Bacteria were collected by centrifugation at 6000*g* for 10 min, washed three times, and resuspended in PBS. Bacterial counts were determined by making dilutions of bacterial suspension, culturing them on LB agar plates at 37°C overnight, and counting the CFUs.

Preparation of coated bacteria

The deposition of $CaCO_3$ was performed on the surface of bacterial cells by mineralization. Briefly, 1×10^8 cells of bacteria were dispersed in 1.5 ml of deionized water containing PVP (2 mg/ml), and 0.2 ml of $CaCl_2$ (0.33 M) was added into bacterial suspension at room temperature. After stirring for 20 min, an equal volume of 0.33 M aqueous Na_2CO_3 was added in the mixture. After stirring for 1 hour, mineralized bacteria were separated by centrifugation (10,000 rpm, 1 min) and washed by PBS three times.

Characterization of coated bacteria

TEM (HITACH, Japan) was used to visualize the morphology of native bacteria and coated bacteria. A drop of sample solution was deposited onto a carbon-coated copper grid and then washed with double-distilled H_2O (ddH_2O) twice (each of them lasted for 5 min). Subsequently, the sample was dried completely in air at room temperature before observation. SEM (ZEISS 1550VP FESEM) was used to visualize the morphology of native bacteria and coated bacteria. Bacteria collected by centrifugation (4000*g*, 5 min) were washed with PBS three times and immediately fixed in 3% glutaraldehyde solution for 1 hour at room temperature. The fixed bacteria were washed twice by PBS and serially dehydrated in 30, 50, 70, 80, 90, and 100% ethanol for 15 min. The

dehydrated samples were dried in air before observation. FTIR (Bruker Tensor 27 spectrometer, USA) was used to examine the surface infrared signals of native and coated bacteria. The samples were collected by centrifugation (4000*g*, 5 min) and rinsed with ddH_2O twice. The obtained samples were freeze-dried for 12 hours. Infrared spectra of samples and background were recorded using a KBr pressed-disk technique within the range of 450 to 4000 cm^{-1} using a resolution of 4 cm^{-1}. For each FTIR spectrum, 64 scans were collected and averaged for each sample and background under certain conditions. For microscopic observation, bacteria were coated with a calcein-labeled mineral layer. In detail, 1×10^8 CFUs of bacteria were dispersed in deionized water containing 10 mM PVP, and 0.2 ml of $CaCl_2$ (0.33 M) was added into bacterial suspension at room temperature. Following 20-min stirring, an equal volume of Na_2CO_3 (330 μM):calcein (0.3 μM) (20:1) was added in the mixture. After 1 hour of stirring, mineralized bacteria were separated by centrifugation (11,300*g*, 1 min) and washed by PBS three times. The labeled coated bacteria were diluted in PBS to appropriate concentrations, which were dropped onto agar gel on a glass slide and covered with glass microscope slides. The obtained samples were observed by LSCM (Leica TCS SP8, German). The zeta potential of mineralized bacteria was examined by DLS (Malvern Zetasizer nano ZS, UK). Coated bacteria labeled with calcein were determined by flow cytometry (Beckman CytoFlex, USA). Native bacteria were used as a control. The gastrointestinal tracts of mice were imaged by IVIS (INIS Lumina II, Caliper).

Growth curves of coated BF839

The cultured bacteria were collected by centrifugation (4000*g*, 5 min) and rinsed with PBS before mineralization as described in the "Preparation of coated bacteria" section. Native BF839, coated BF839, and decoated BF839 were separately diluted to reach an OD_{600} value of 0.15 in GAM and incubated at 37°C with gently shaking. The OD_{600} value of the cultures was recorded by a microplate reader (BioTek, USA) at 0.5-hour intervals in 96-well plates for 12 hours.

In vitro gastric acid neutralization

In vitro study of gastric acid neutralization was performed by measuring the pH value of SGF (pH 1.2) with a pH meter (Mettler Toledo, Columbus, OH, USA). After adding an equal number of coated bacteria (1×10^8 CFUs) into 20 ml of SGF at 1-min intervals, the change of pH value was recorded at room temperature.

Resistance assay of coated BF839 against environmental insults

Equal amounts of coated BF839 and native BF839 were exposed to air for storage at 4°C for 30 days or exposed to UV radiation for 30 min with 100 μW/cm^2. It is reported that the surface can be sterilized under an UV radiance of 10 μW/cm^2 (*53*). Meanwhile, equal amounts of coated BF839 and native BF839 were resuspended into 1 ml of medium supplemented with 75% ethanol and incubated at 37°C with gently shaking. At predetermined time points, 50 μl of each sample was taken out, washed with fresh PBS, serially diluted with PBS, and spread on agar plates. The colonies were counted after incubating at 37°C overnight. Samples were withdrawn at predetermined time periods and observed by TEM.

Gastrointestinal retention of coated bacteria

Female ICR mice (6 to 8 weeks, 17 to 20 g) were used to evaluate the retention of coated bacteria in the gastrointestinal tract. The plasmids pBBR1MCS2-Tac-mCherry and pMD18-luxCDABE were electrotransformed into EcN using the reported method with modifications (*54*), respectively. As follows, EcN grown in LB medium to an OD_{600} of 0.9 to 1.0 were placed in an ice bath for 15 min. Then, bacteria were resuspended in glycerol (10%) and centrifuged for 15 min at 5000*g* (4°C). Bacterial cells were resuspended in electroporation buffer (0.075% peptone, 0.038% yeast extract, and 10% glycerol), and the plasmid of pBBR1MCS2-Tac-mCherry or pMD18-luxCDABE (1 μg) was dropped into 50 μl of bacterial resuspension. The suspension was electroporated at 1.2 kV, obtaining a time constant of 4.5 to 5 ms. Last, transformant was selected in LB agar added with kanamycin or ampicillin. After obtaining mCherry- or LuxCDABE-expressed EcN, a number of 1×10^7 CFUs of native or coated EcN were administered by oral gavage. EcN expressing mCherry were coated with calcein-labeled mineral layer. The mice were euthanized at 0, 1, and 5 hours after administration, respectively. The contents in the gastrointestinal tract, including the stomach and intestine, were serially diluted with PBS. A volume of 50 μl of each dilution was spread onto solid GAM agar plates, which were further incubated at 37°C for 12 hours before counting. The survivals in gastrointestinal tract were also observed by the IVIS system at 1 and 5 hours after oral gavage of native EcN expressing LuxCDABE or EcN coated with a calcein-labeled mineral layer.

DSS-induced mouse model of colitis

C57BL/6 female mice at 6 to 8 weeks of age were given with 3% DSS salt (molecular weight of 36,000 to 50,000 kDa; Sangon, China) in sterile drinking water for 7 days. Then, the mice were randomly divided to different groups and orally administered with native BF839 or coated BF839 (1×10^7 CFUs per mouse per day) or PBS for another 5 days. Healthy mice without treatment were used as a control. The weight of mice was measured every day, and then the mice were euthanized by asphyxia with CO_2. One milliliter of blood from each mouse was collected and stored in a 1.5ml Eppendorf tube and then incubated at 37°C for 30 min. The serum of each mouse was isolated by centrifugation of the collected blood at 4000*g* for 5 min and then assayed to determine the concentration of TNF-α using ELISA kits (MultiSciences Biotech, China). The colons were harvested for length measurement and lastly fixed in 4% formalin for blinded histopathology analysis.

Histopathology analysis

The colon samples were fixed in 4% formalin, processed according to a defined procedure for paraffin embedding. The paraffin-embedded samples were sectioned at 4 μm, and then H&E staining and MPO staining were performed. The samples were scanned by 3D HISTECH Pannoramic 250 (3DHISTECH, Hungary). To detect MPO expression, a two-step immunostaining technique was used. Tissue sections were firstly dewaxed and immersed in 3% H_2O_2 in methanol for 30 min. After heating in a microwave for 20 min, the tissue sections were washed with PBS and incubated overnight with primary MPO antibody (Boster Biological Technology Ltd.) at 4°C. After washing with PBS, diaminobenzidine was added as a chromogen to terminate peroxidase reactions. The counting of MPO-positive cells in brown was performed by an experienced pathologist,

who was blinded to the samples. Scores were given on the basis of reported methods (*55*).

Statistical analysis

All data were presented as means ± SD. Statistical analysis was performed using Prism 8.0 (GraphPad, USA). The results were analyzed with one-way analysis of variance (ANOVA) with the least significance difference test among three groups. Unpaired two-tailed Student's *t* test was used for comparison between two groups. Differences were considered statistically significant if $P < 0.05$ ($^{*}P < 0.05$, $^{**}P < 0.01$, $^{***}P < 0.001$, and $^{****}P < 0.0001$).

Supplementary Materials

This PDF file includes:

Figs. S1 to S9

View/request a protocol for this paper from *Bio-protocol*.

REFERENCES AND NOTES

1. Y. Fu, Y. Wang, H. Gao, D. Li, R. Jiang, L. Ge, C. Tong, K. Xu, Associations among dietary omega-3 polyunsaturated fatty acids, the gut microbiota, and intestinal immunity. *Mediators Inflamm.* **2021**, 8879227 (2021).
2. J. Palmu, L. Lahti, T. Niiranen, Targeting gut microbiota to treat hypertension: A systematic review. *Int. J. Environ. Res. Public Health* **18**, 1248 (2021).
3. L. Liu, X. Ni, T. Tian, X. Li, F. Li, M. Sun, J. Chen, S. Zhou, L. Zhao, Effect of regulating gut microbiota using probiotics on functional changes in the brain: protocol for a systematic review. *BMJ Open* **10**, e037582 (2020).
4. A. C. Anselmo, Y. Gokarn, S. Mitragotri, Non-invasive delivery strategies for biologics. *Nat. Rev. Drug Discov.* **18**, 19–40 (2019).
5. G. Fan, P. Wasuwanich, M. R. Rodriguez-Otero, A. L. Furst, Protection of anaerobic microbes from processing stressors using metal-phenolic networks. *J. Am. Chem. Soc.* **144**, 2438–2443 (2022).
6. W. Li, L. Liu, H. Tian, X. Luo, S. Liu, Encapsulation of Lactobacillus plantarum in cellulose based microgel with controlled release behavior and increased long-term storage stability. *Carbohydr. Polym.* **223**, 115065 (2019).
7. P. Kanmani, R. S. Kumar, N. Yuvaraj, K. A. Paari, V. Pattukumar, V. Arul, Cryopreservation and microencapsulation of a probiotic in alginate-chitosan capsules improves survival in simulated gastrointestinal conditions. *Biotechnol. Bioprocess Eng.* **16**, 1106–1114 (2011).
8. D. W. Zheng, P. Pan, K. W. Chen, J. X. Fan, C. X. Li, H. Cheng, X. Z. Zhang, An orally delivered microbial cocktail for the removal of nitrogenous metabolic waste in animal models of kidney failure. *Nat. Biomed. Eng.* **4**, 853–862 (2020).
9. A. M. Vargason, S. Santhosh, A. C. Anselmo, Surface modifications for improved delivery and function of therapeutic bacteria. *Small* **16**, 2001705 (2020).
10. A. M. Urbanska, J. Bhathena, S. Prakash, Live encapsulated Lactobacillus acidophilus cells in yogurt for therapeutic oral delivery: Preparation and in vitro analysis of alginate-chitosan microcapsules. *Can. J. Physiol. Pharmacol.* **85**, 884–893 (2007).
11. X. Yang, J. Yang, Z. Ye, G. Zhang, W. Nie, H. Cheng, M. Peng, K. Zhang, J. Liu, Z. Zhang, J. Shi, Physiologically inspired mucin coated Escherichia coli Nissle 1917 enhances biotherapy by regulating the pathological microenvironment to improve intestinal colonization. *ACS Nano* **16**, 4041–4058 (2022).
12. J. Liu, W. Li, Y. Wang, Y. Ding, A. Lee, Q. Hu, Biomaterials coating for on-demand bacteria delivery: Selective release, adhesion, and detachment. *Nano Today* **41**, 101291 (2021).
13. F. Centurion, A. W. Basit, J. Liu, S. Gaisford, M. A. Rahim, K. Kalantar-Zadeh, Nanoencapsulation for probiotic delivery. *ACS Nano* **15**, 18653–18660 (2021).
14. B. J. Kim, H. Cho, J. H. Park, J. F. Mano, I. S. Choi, Strategic advances in formation of cell-in-shell structures: From syntheses to applications. *Adv. Mater.* **30**, 1706063 (2018).
15. S. Lin, S. Mukherjee, J. Li, W. Hou, C. Pan, J. Liu, Mucosal immunity–mediated modulation of the gut microbiome by oral delivery of probiotics into Peyer's patches. *Sci. Adv.* **7**, eabf0677 (2021).
16. X. Wang, Z. Cao, M. Zhang, L. Meng, Z. Ming, J. Liu, Bioinspired oral delivery of gut microbiota by self-coating with biofilms. *Sci. Adv.* **6**, eabb1952 (2020).
17. P. Feng, Z. Cao, X. Wang, J. Li, J. Liu, On-demand bacterial reactivation by restraining within a triggerable nanocoating. *Adv. Mater.* **32**, 2002406 (2020).
18. C. Pan, J. Li, W. Hou, S. Lin, L. Wang, Y. Pang, Y. Wang, J. Liu, Polymerization-mediated multifunctionalization of living cells for enhanced cell-based therapy. *Adv. Mater.* **33**, 2007379 (2021).
19. L. L. Tan, M. Mahotra, S. Y. Chan, S. C. J. Loo, In situ alginate crosslinking during spray-drying of lactobacilli probiotics promotes gastrointestinal-targeted delivery. *Carbohydr. Polym.* **286**, 119279 (2022).
20. J. Pan, G. Gong, Q. Wang, J. Shang, Y. He, C. Catania, D. Birnbaum, Y. Li, Z. Jia, Y. Zhang, N. S. Joshi, J. Guo, A single-cell nanocoating of probiotics for enhanced amelioration of antibiotic-associated diarrhea. *Nat. Commun.* **13**, 2117 (2022).
21. Z. Cao, X. Wang, Y. Pang, S. Cheng, J. Liu, Biointerfacial self-assembly generates lipid membrane coated bacteria for enhanced oral delivery and treatment. *Nat. Commun.* **10**, 5783 (2019).
22. Z. Lu, J. A. Imlay, When anaerobes encounter oxygen: mechanisms of oxygen toxicity, tolerance and defence. *Nat. Rev. Microbiol.* **19**, 774–785 (2021).
23. A. Dafe, H. Etemadi, A. Dilmaghani, G. R. Mahdavinia, Investigation of pectin/starch hydrogel as a carrier for oral delivery of probiotic bacteria. *Int. J. Biol. Macromol.* **97**, 536–543 (2017).
24. N. Asaithambi, S. K. Singh, P. Singha, Current status of non-thermal processing of probiotic foods: A review. *J. Food Eng.* **303**, 110567 (2021).
25. M. Gu, Z. Zhang, C. Pan, T. R. Goulette, R. Zhang, G. Hendricks, D. J. McClements, H. Xiao, Encapsulation of Bifidobacterium pseudocatenulatum G7 in gastroprotective microgels: Improvement of the bacterial viability under simulated gastrointestinal conditions. *Food Hydrocoll.* **91**, 283–289 (2019).
26. G. Luz, J. Mano, Mineralized structures in nature: Examples and inspirations for the design of new composite materials and biomaterials. *Compos. Sci. Technol* **70**, 1777–1788 (2010).
27. W. Wang, X. Liu, X. Zheng, H. J. Jin, X. Li, Biomineralization: An opportunity and challenge of nanoparticle drug delivery systems for cancer therapy. *Adv. Healthc. Mater.* **9**, 2001117 (2020).
28. Y. Guo, Z. Xu, M. Liu, S. Zu, Y. Yang, Q. Wang, Z. Yu, Z. Zhang, L. Ren, The corrosion resistance, biocompatibility and biomineralization of the dicalcium phosphate dihydrate coating on the surface of the additively manufactured NiTi alloy. *J. Mater. Res. Technol.* **17**, 622–635 (2022).
29. D. Qu, F. Sun, S. Feng, L. Yu, F. Tian, H. Zhang, W. Chen, Q. Zhai, Protective effects of Bacteroides fragilis against lipopolysaccharide-induced systemic inflammation and their potential functional genes. *Food Funct.* **13**, 1015–1025 (2022).
30. S. Zhang, K. E. Gonsalves, Influence of the chitosan surface profile on the nucleation and growth of calcium carbonate films. *Langmuir* **14**, 6761–6766 (1998).
31. Q. Li, A. Fernandez-Martinez, B. Lee, G. A. Waychunas, Y. S. Jun, Interfacial energies for heterogeneous nucleation of calcium carbonate on mica and quartz. *Environ. Sci. Technol.* **48**, 5745–5753 (2014).
32. Y. Ohno, A. Iguchi, C. Shinzato, M. Gushi, M. Inoue, A. Suzuki, K. Sakai, T. Nakamura, Calcification process dynamics in coral primary polyps as observed using a calcein incubation method. *Biochem. Biophys. Rep.* **9**, 289–294 (2017).
33. M. Hecker, U. Völker, General stress response of *Bacillus subtilis* and other bacteria, in *Advances in Microbial Physiology*, Robert Poole, Ed. (Academic Press, 2001), vol. 44, pp. 35–91.
34. R. D. Rolfe, D. J. Hentges, J. T. Barrett, B. J. Campbell, Oxygen tolerance of human intestinal anaerobes. *Am. J. Clin. Nutr.* **30**, 1762–1769 (1977).
35. T. P. Silva, J. P. Gamalier, N. Resende, N. Barros, R. Melo, Microscopy techniques applied to the study of cell death in bacteria from freshwater ecosystems, in *Microscopy and Imaging Science: Practical Approaches to Applied Research and Education*, A. Méndez-Vilas, Ed. (Formatex Research Center, 2017), pp. 253–259.
36. Z. Ji, H. Zhang, H. Liu, O. M. Yaghi, P. Yang, Cytoprotective metal-organic frameworks for anaerobic bacteria. *Proc. Natl. Acad. Sci. U.S.A.* **115**, 10582–10587 (2018).
37. E. Khoori, V. Hakimzadeh, A. Mohammadi Sani, H. Rashidi, Effect of ozonation, UV light radiation, and pulsed electric field processes on the reduction of total aflatoxin and aflatoxin M1 in acidophilus milk. *J. Food Process. Preserv.* **44**, e14729 (2020).
38. M. M. Delorme, J. T. Guimarães, N. M. Coutinho, C. F. Balthazar, R. S. Rocha, R. Silva, L. P. Margalho, T. C. Pimentel, M. C. Silva, M. Q. Freitas, D. Granato, A. S. Sant'Ana, M. C. K. H. Duart, A. G. Cruz, Ultraviolet radiation: An interesting technology to preserve quality and safety of milk and dairy foods. *Trends Food Sci. Technol.* **102**, 146–154 (2020).
39. G. Invernizzi, L. Casiraghi, R. Grandori, M. Lotti, Deactivation and unfolding are uncoupled in a bacterial lipase exposed to heat, low pH and organic solvents. *J. Biotechnol.* **141**, 42–46 (2009).
40. H. E. Morton, The relationship of concentration and germicidal efficiency of ethyl alcohol. *Ann. N. Y. Acad. Sci.* **53**, 191–196 (1950).
41. S. Razavi, S. Janfaza, N. Tasnim, D. L. Gibson, M. Hoorfar, Nanomaterial-based encapsulation for controlled gastrointestinal delivery of viable probiotic bacteria. *Nanoscale Adv.* **3**, 2699–2709 (2021).

42. Z. Cao, S. Cheng, X. Wang, Y. Pang, J. Liu, Camouflaging bacteria by wrapping with cell membranes. *Nat. Commun.* **10**, 3452 (2019).
43. J.-W. Kang, H.-Y. Lee, D.-H. Kang, Synergistic bactericidal effect of hot water with citric acid against Escherichia coli O157:H7 biofilm formed on stainless steel. *Food Microbiol.* **95**, 103676 (2021).
44. A. A. D'Archivio, L. Galantini, E. Gavuzzo, E. Giglio, F. Mazza, Calcium ion binding to bile salts. *Langmuir* **13**, 3090–3095 (1997).
45. J. M. Landete, M. Medina, J. L. Arqués, Fluorescent reporter systems for tracking probiotic lactic acid bacteria and bifidobacteria. *World J. Microbiol. Biotechnol.* **32**, 119 (2016).
46. S. Chen, K. Zhu, R. Wang, X. Zhao, Preventive effect of polysaccharides from the large yellow croaker swim bladder on HCl/ethanol induced gastric injury in mice. *Exp. Ther. Med.* **8**, 316–322 (2014).
47. J. Torres, S. Mehandru, J.-F. Colombel, L. Peyrin-Biroulet, Crohn's disease. *Lancet* **389**, 1741–1755 (2017).
48. S. Zhang, J. Ermann, M. D. Succi, A. Zhou, M. J. Hamilton, B. Cao, J. R. Korzenik, J. N. Glickman, P. K. Vemula, L. H. Glimcher, G. Traverso, R. Langer, J. M. Karp, An inflammation-targeting hydrogel for local drug delivery in inflammatory bowel disease. *Sci. Transl. Med.* **7**, 300ra128 (2015).
49. C. Wang, S. Li, K. Hong, L. Yu, F. Tian, J. Zhao, H. Zhang, W. Chen, Q. Zhai, The roles of different *Bacteroides fragilis* strains in protecting against DSS-induced ulcerative colitis and related functional genes. *Food Funct* **12**, 8300–8313 (2021).
50. S. Sánchez-Fidalgo, L. Sánchez de Ibargüen, A. Cárdeno, C. Alarcón de la Lastra, Influence of extra virgin olive oil diet enriched with hydroxytyrosol in a chronic DSS colitis model. *Eur. J. Nutr.* **51**, 497–506 (2012).
51. M. K. Moon, B. J. Cho, Y. J. Lee, S. H. Choi, S. Lim, K. S. Park, Y. J. Park, H. C. Jang, The effects of chronic exercise on the inflammatory cytokines interleukin-6 and tumor necrosis factor-α are different with age. *Appl. Physiol. Nutr. Metab.* **37**, 631–636 (2012).
52. W. A. Goodman, S. M. Bedoyan, H. L. Havran, B. Richardson, M. J. Cameron, T. T. Pizarro, Impaired estrogen signaling underlies regulatory T cell loss-of-function in the chronically inflamed intestine. *Proc. Natl. Acad. Sci. U.S.A.* **117**, 17166–17176 (2020).
53. W. Kowalski, *Ultraviolet Germicidal Irradiation Handbook* (Springer Science & Business Media, 2009).
54. L. Cao, L. Pan, L. Gong, Y. Yang, H. He, Y. Li, Y. Peng, D. Li, L. Yan, X. Ding, S. Hu, Z. Yu, Y. Sun, W. Huang, Y. Hu, G. Yi, L. Xia, Interaction of a novel Bacillus velezensis (BvL03) against Aeromonas hydrophila in vitro and in vivo in grass carp. *Appl. Microbiol. Biotechnol.* **103**, 8987–8999 (2019).
55. Z. Zeng, L. Zhan, H. Liao, L. Chen, X. Lv, Curcumin improves TNBS-induced colitis in rats by inhibiting IL-27 expression via the TLR4/NF-κB signaling pathway. *Planta Med.* **79**, 102–109 (2013).

Acknowledgments

Funding: This work was supported by the National Key Research and Development Program of China (2021YFA0909400), the National Natural Science Foundation of China (22275105, 32101218, and 22105123), the Foundation of National Infrastructures for Translational Medicine (Shanghai) (TMSK-2021-119), and the Innovative Research Team of High-Level Local Universities in Shanghai (SHSMU-ZDCX20210900). **Author contributions:** J.L. supervised the project. J.L. conceived and designed the experiments with Z.G., F.W., and Z.C. Z.G., X.W., F.W., and Z.C. performed all experiments. All authors analyzed and discussed the data. Z.G. and J.L. wrote the paper. **Competing interests:** J.L. and Z.G. are inventors on a pending patent application related to this work (no. 2022116072610.0, filed 14 December 2022). The authors declare that they have no other competing interests. **Data and materials availability:** All data needed to evaluate the conclusions in the paper are present in the paper and/or the Supplementary Materials.

Submitted 25 July 2022
Accepted 9 February 2023
Published 17 March 2023
10.1126/sciadv.ade0997